Nano Scale Disruptive Silicon-Plasmonic Platform for Chip-to-Chip Interconnection

Designs of plasmonic amplifiers

Deliverable no.:	D4.1
Due date:	04/30/2013
Actual Submission date:	05/31/2013
Authors:	AIT
Work package(s):	WP4
Distribution level:	RE[1] (NAVOLCHI Consortium)
	Nature: document, available online in the restricted area of the NAVOLCHI webpage

List of Partners concerned

Partner number	Partner name	Partner short name	Country	Date enter project	Date exit project
2	INTERUNIVERSITAIR MICRO-ELECTRONICA CENTRUM VZW	IMEC	Belgium	M1	M36
4	RESEARCH AND EDUCATION LABORATORY IN INFORMATION TECHNOLOGIES	AIT	Greece	M1	M36
5	UNIVERSITAT DE VALENCIA	UVEG	Spain	M1	M36
7	UNIVERSITEIT GENT	UGent	Belgium	M1	M36

[1] **PU** = Public
PP = Restricted to other programme participants (including the Commission Services)
RE = Restricted to a group specified by the consortium (including the Commission Services)
CO = Confidential, only for members of the consortium (including the Commission Services)

Deliverable Responsible

Organization: Athens Information Technology
Contact Person: Emmanouil-P. Fitrakis
Address: Athens Information Technology
19.5 Km Markopoulo Avenue,
19002 Peania, Attiki, Greece
Phone: +30 210 6682721
E-mail: mfitrakis@ait.gr

Executive Summary

This report deals with the design of planar plasmonic amplifiers based on QD-PMMA nanocomposite and silicon-plasmonic hybrid structures. Studies have been carried out both in the visible and the infrared and initial experimental results have been included. Regarding the QD-PMMA nanocomposite structures, a symmetric PMMA/Au/PMMA with a bilayer cladding on top has been chosen as the optimal solution in the context of NAVOLCHI. Also, silicon-plasmonic hybrid structures are currently being fabricated.

Change Records

Version	Date	Changes	Author
0.1 (draft)	2013-03-20	Start	Isaac Suárez
0.2 (draft)	2013-04-30	draft	Emmanouil Fitrakis Isaac Suarez Juan Martinez-Pastor Ioannis Tomkos Dries Van Thourhout
1.1 (subm.)	2013-05-31	submission	Emmanouil Fitrakis Ioannis Tomkos Isaac Suarez Juan Martinez-Pastor Dries Van Thourhout

Contents

1. Introduction and objectives

Surface plasmons (SP) are coherent oscillations of free electrons present at the boundary between a metal and a dielectric. Under appropriate conditions when SPs are exposed to a flow of visible or infrared light, such oscillations can be coupled to the incident photons leading to a hybrid electromagnetic-wave and surface-charge state known as surface plasmon polariton (SPP). In these conditions SPP can propagate along the interface showing unique properties as subwavelength confinement, strong near electromagnetic field enhancement or high sensitivity to the environment [1]. However, the ohmic losses present in the metal lead to the strong attenuation of the electromagnetic wave, limiting the propagation length of SPP (see figure 1a) and, in consequence, the potential applications. Indeed, strong enough mode confinement, necessary for exploiting the possibility of guiding light beyond the diffraction limit, is achieved using thick metal layers, even if propagation losses of SPP increase with the metal thickness, so there is a trade-off between good mode confinement and low propagation losses [2]. This problem can be surpassed by providing gain in the dielectric material adjacent to the metal, and hence absorption losses can be compensated and the SPP propagation length can be significantly increased (see illustration in figure 1b). In literature, different materials like dyes [3], fluorescent polymers [4], rare earths [5] and PbSe quantum dots [6] have been proposed as gain media for wavelengths between 600 and 1500 nm.

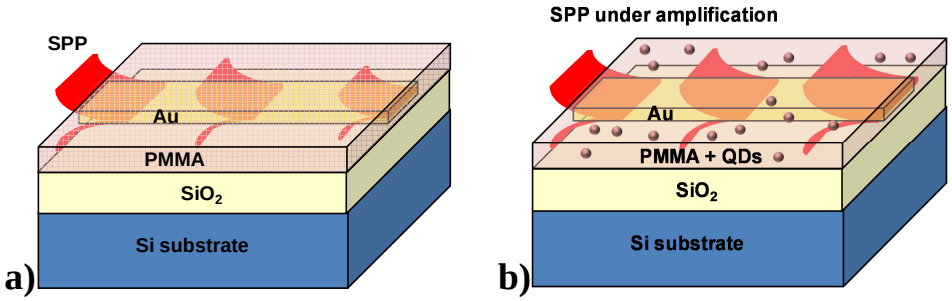

Figure 1. Structure of the surface plasmon polariton waveguide and propagation without (a) and with amplification (b).

In this project, the amplifier concept is pursued by two Si-compatible approaches and using colloidal quantum dots (QD) as the gain medium. QDs are semiconductor nanocrystals synthetized by colloidal chemistry and have the advantages of high emission efficiency at room temperature and color tuning by size and base material.

In the first approach, a novel material based on the incorporation of colloidal quantum dots in a polymer matrix is proposed as a dielectric medium to provide gain in plasmonic waveguides. This kind of nanocomposite (polymer + quantum dots) is useful because it combines the tunable optical properties of colloidal quantum dots together with the technological feasibility of polymers (spin coating, UV and e-beam lithography). Indeed, the application of CdSe/PMMA in the development of active dielectric waveguides has already been demonstrated at 600 nm [7-8] by depositing the nanocomposite on a SiO_2/Si substrate. In this project, we proposed the use of QD-PMMA (and/or QD-SU8) nanocomposites onto a gold layer or stripe able to provide gain in the SPP travelling through the metal when the nanocomposite is optically pumped. Different designs using metal films have been studied. Also, since the operation wavelength can be tuned just by changing the QD material, preliminary tests *at* λ*=600 nm* (CdSe) have been performed, given that this is the most studied

QD-material in literature, and then the conclusions obtained have been extrapolated to PbS or PbSe QDs, and other nanostructures emitting at infrared wavelengths.

The second approach is also based on the use of infrared emitting QDs, but now using patterned silicon waveguides and electrical injection on a silicon-on-insulator (SOI) platform. In this way, we will extend the capabilities of this platform (CMOS fabrication compatibility) to include plasmonics and active photonics. For this purpose, we propose a hybrid platform where standard SOI waveguides are covered with an active layer (e.g. for modulation or light generation) and a cathode layer (for electrical contacting). Since silicon is conducting (or can be made so by p/n-doping) we can use the waveguide itself as the anode contact, whereas the cathode can be an appropriate metal (Au), or highly doped semiconductor (a-Si), in order to influence the confinement of the optical mode in the SOI waveguide, other than serving as electrode for producing carrier injection at the QD layer.

Therefore, both approaches are being developed in parallel on a CMOS compatible substrate, as the others devices of the project. In this report, we summarize the advances obtained in the plasmonic amplifier configuration and preliminary experimental results.

a. Planar amplifiers

In a first approximation, the conditions for light coupling, SPP propagation and SPP amplification have been thoroughly studied in planar plasmonic waveguides. Figure 2 shows the three structures analyzed in this work. The first design (figure 2a) consists of a gold layer evaporated on a SiO_2/Si substrate and a nanocomposite (QD-PMMA) film spin-coated on the top of the structure. In the second waveguide (figure 2b) the gold layer is evaporated between two nanocomposite films. In both cases the thickness of the SiO_2 was fixed to 2 µm, because it is the thickness provided by the wafer supplier, and thick enough to isolate the PMMA/Au and PMMA/Au/PMMA layers from the silicon for infrared wavelengths. The thicknesses of the gold layer (t) and nanocomposite films (d, d_1, d_2) are the parameters to be optimized in the theoretical design work. Also, the concentration of nanoparticles inside the polymer is another critical factor that has been experimentally studied. Finally, a design that consists of a bilayer structure on the top of the gold is also proposed (see figure 2c). This bilayer structure is composed by a thin active layer and a thick passive one, and has the advantages of optimizing the overlap of the SPP with the active material and allowing a better coupling of the pump beam; the thicknesses of the top bilayer (d_1 and d_3) have been properly optimized.

Finally, it is important to mention that the optimization has a critical dependence on the operation wavelength. So, two different working wavelengths were considered: 600 and 1550 nm. A couple of reasons were considered to start the work at 600 nm: i) we were preparing our set-ups for optical characterization of waveguides and amplifier devices at 1550 nm and ii) we could compare our findings at visible wavelengths with literature, mostly centered on using CdSe QDs and organic dyes [3-4] (only a small number of works propose losses compensation in the IR [5-6]). The conclusions of this preliminary work have been extrapolated and served to shorten the design workload at 1550 nm, the target of the project. .

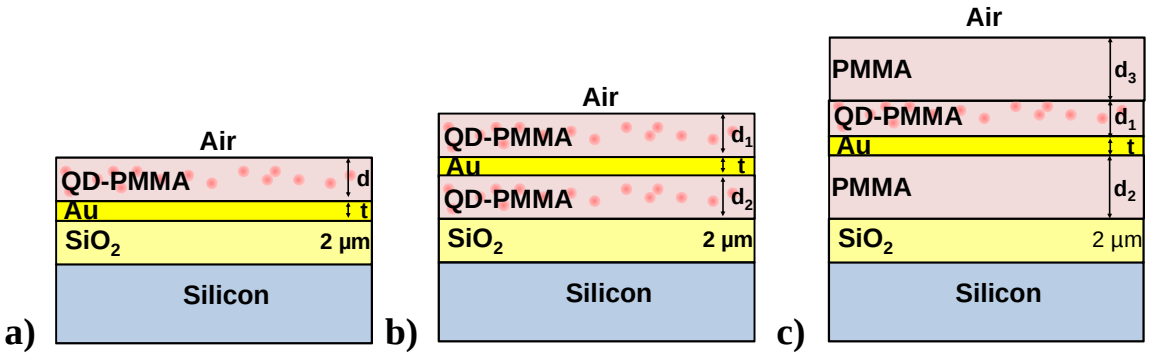

Figure 2. Designs of planar plasmonic amplifiers.

b. 2-D amplifiers

In order to improve the confinement of the light, bidimensional waveguides like the ones shown in figure 3 are proposed as well. The first one (figure 3a) consists of a dielectric stripe on the top of the gold layer. This structure is called dielectric loaded waveguide and it is interesting for optical interconnects because it allows a reduction of the SPP propagation losses. Due to the fact that the PMMA doesn't have lithographic properties, SU-8 is chosen as dielectric material. The second kind of waveguides (figure 3 b) is composed of gold stripes embedded into the QD-PMMA nanocomposite, and hence achieves a 2-D confinement of the SPP. Finally, a structure like the one shown in figure 3c is also proposed. The idea is similar to the one depicted in figure 2c, but includes patterning the passive material in the top bilayer structure.

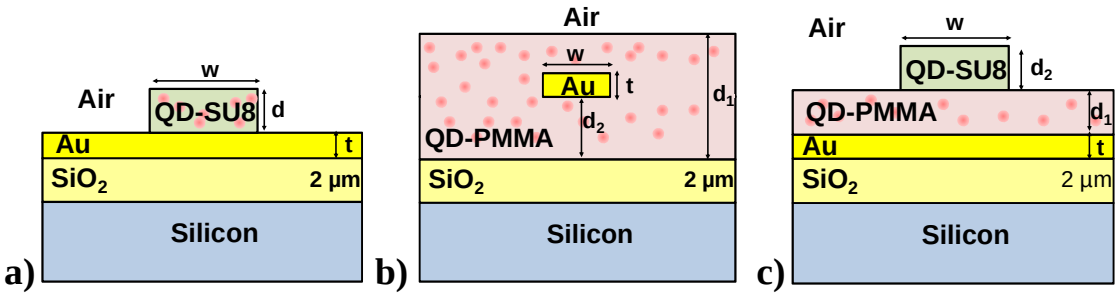

Figure 3. Designs of 2D plasmonic amplifiers.

c. Experimental considerations

c.1. Nanostructures.

Figures 4a and 4b show the absorption and photoluminiscence (PL) spectra of the CdSe and PbS QDs used in this work. The PL line of CdSe QDs is centered at 620 nm and has a Full Width at Half Maximum (FWHM) of 40 nm. The absorbance peak corresponding to the ground state exciton transition is measured at 580 nm, whereas an excited state transition is observed at around 480 nm. Concerning the PbS, the PL is centered at 1550 nm and the absorption exciton peak close to 1500 nm.

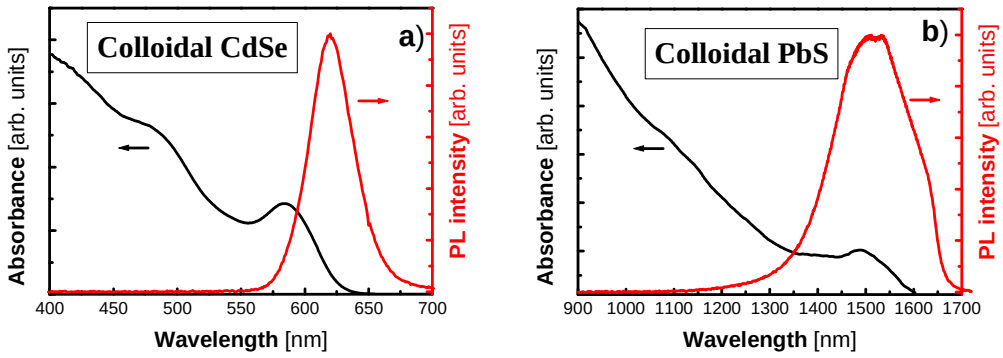

Figure 4. Absorbance (black line) and PL (red line) spectra of CdSe and PbS used in this work.

The limitation of this kind of spherical QDs is the reduced Stokes shift between absorption and PL spectra giving rise to reabsorption effects [7]. Then, spherical QDs are good as a proof of concept for SPP excitation and propagation mode analysis, but they are not practical for amplification purposes. From this point of view, other nanostructures seem to be a better approach. For example, in this work some results using PbS-CdS partially exchanged rods will be also included, because these nanostructures exhibit a long Stokes-shift and, in consequence, better gain/losses ratios.

c.2. Materials and sample fabrication.

The samples are implemented as follows. Nanocomposites were fabricated by mixing the PMMA and the QDs solution in an appropriate proportion. Then, they are deposited on the gold or the SiO_2 by spin coating between 3000 and 5000 rpm and baking at 80 ºC and 150 ºC during 2 minutes. PMMA is deposited in the same way. Concerning the Au layers, they are deposited on PMMA or SiO_2 by evaporation. Table I shows the refractive index at the wavelengths of interest. It is important to note that the filling factor (*ff*) of QDs in PMMA is low enough (~10^{-3}) to consider its refractive index equal to the one of PMMA.

Material	600 nm	1550 nm
Air	1	1
SiO_2	1.4582	1.4522
PMMA	1.489	1.483
Au	0.2203-3i	0.439-9.519i
Si	3.9359-0.0193i	3.6401-0.0036i

Table I. Material's refractive indices

c.3. Experimental set ups.

Figure 5 shows the experimental set-ups used to characterize the samples. The set-up shown in figure 5a consists of the standard end fire coupling system where an input beam

is coupled from one edge of the sample with the aid a microscope objective, and the light at the output is collected with another microscope objective that can focus it into a CCD camera or a spectrograph. If the wavelength of the pump beam is short enough to pump efficiently the QDs, they will produce waveguided PL through the structure together with the pumping beam propagation. At the output of the system a high pass filter is included in order to separate both signals, PL and pump beam. However, the design shown in figure 2b is difficult to be characterized with this set-up, because the strong attenuation in the gold layer will limit the propagation length of the SPP modes in the range 10-100 µm, and samples with such a length are difficult to fabricate and manipulate. The set-up shown in figure 5b avoids this problem. It consists of focusing the pump beam as a straight line (using a cylindrical lens) on the top surface of the sample. In order to avoid the influence of the Gaussian profile of the laser, a slit was used to keep the central 1.4 mm of the beam, where its intensity is approximately constant and hence the QDs will be homogeneously excited along the waveguide structure. Then the propagation of the waveguided PL signal will follow the equation:

$$\frac{dI_v(x)}{dx} = I_{SS} + (g - \alpha) \cdot I_v(x), \quad (1)$$

where I_v is the intensity of the light, I_{SS} the intensity of the spontaneous emission, g the gain and α the losses. The gain of the structure can be estimated by measuring the emission intensity, $I_v(d)$, as a function of the pumping strip length (d) by the variable stripe length (VSL) method [9]. When saturation is absent, the gain of the structure can be deduced from:

$$I_v(d) = \frac{I_{SS}}{g-\alpha} \cdot \left(e^{(g-\alpha)\cdot d} - 1\right). \quad (2)$$

However, in the presence of saturation by Auger non radiative recombination, the gain could be expressed by the function [9]:

$$g = g_0 \cdot e^{-d/L}, \quad (3)$$

where g_0 and L are fitting parameters related with the gain and the saturation. Similarly, the attenuation of the waveguide can be characterized by keeping the length of the stripe constant and moving it away from the edge of the sample. Then, propagation losses can be fitted by approximating the dependence of the output intensity as a function of the distance between the stripe and the edge of the sample (x) with an exponential decrease:

$$I(x) \propto e^{-\alpha \cdot x} \quad (4)$$

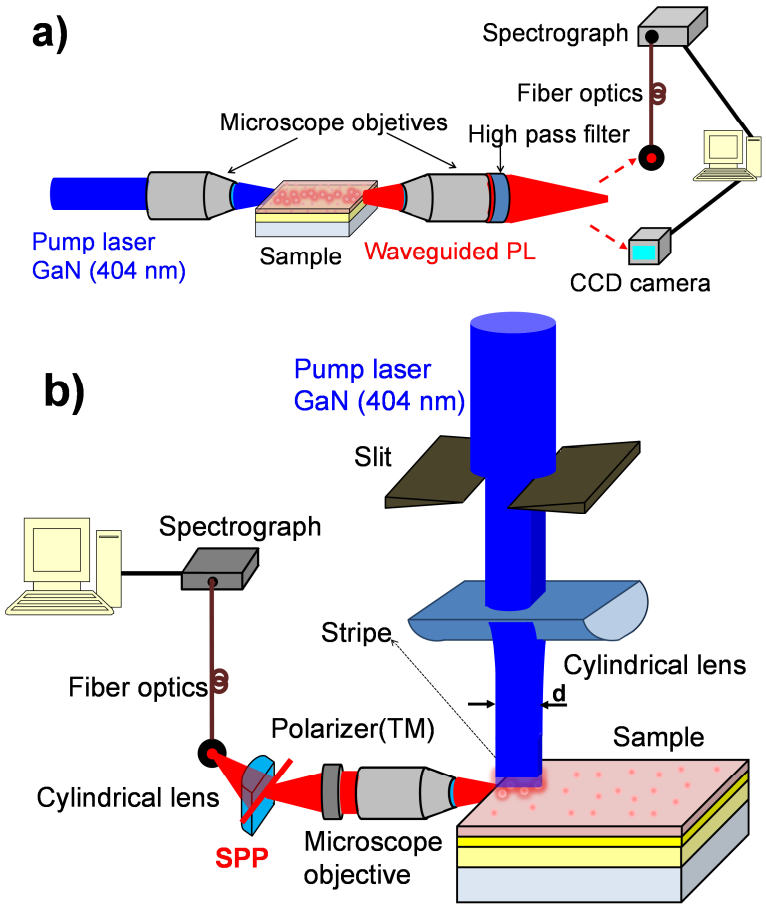

Figure 5. a) Experimental set-up to couple light from the edge of the sample. b) Experimental set-up to optical pumping from the surface

2. Design of planar plasmonic amplifiers at 600 nm.

SPP waveguides have been initially tested at $\lambda=600\ nm$ in order to perform a first optimization of the light coupling set-up and fabrication conditions. Several samples with the three structures shown in figure 2 have been studied, establishing the influence of each fabrication parameter (t, d_1, d_2, d_3) on the propagation characteristics in the plasmonic waveguide. For this purpose, the optical modes in the structures were solved using the transfer matrix method [10] with the refractive indices listed in Table I. It is interesting to note that this kind of waveguides support two plasmonic modes: the long range SPP (LR-SPP) and the short range SPP (SR- SPP). However, the influence of the second mode will be neglected due to the fact that it exhibits a short propagation length and hence the LR-SPP.

a. Three-layer structures

In order to optimize the thickness of the metal (t), waveguides that consist of Au films sandwiched by PMMA/PMMA or PMMA/SiO_2 semi-infinite layers have been simulated. The

metal thickness implies a trade-off between mode confinement and propagation losses [2]: the thicker the Au layer, the better the confinement of the long range SPP (LR-SPP) in the metal. However, thicker layers also imply a reduction in the propagation length due to the attenuation in the metal. Figure 6a plots the propagation length and the LR-SPP confinement as a function of the Au thickness at $\lambda = 600\ nm$. Close and open symbols correspond to the symmetric (PMMA/Au/PMMA) and asymmetric (PMMA/Au/SiO_2) structures, respectively. The LR-SPP mode can achieve confinements up to 10-15 %, but the maximum propagation length is only around 100 µm. Both the symmetric and asymmetric waveguides show similar propagation lengths, but for thick Au layers (t>60 nm) the mode confinement seems to be better in the PMMA/Au/SiO_2 waveguides. For Au thicknesses from 20 to 40 nm a good compromise between losses (represented in log-scale) and confinement is found. Figure 6b shows the power distribution of the LR-SPP mode in the asymmetric structure using $t = 30\ nm$. The mode is centered at the gold layer with an exponential decay of 280 nm at $1/e^2$ in the dielectric medium.

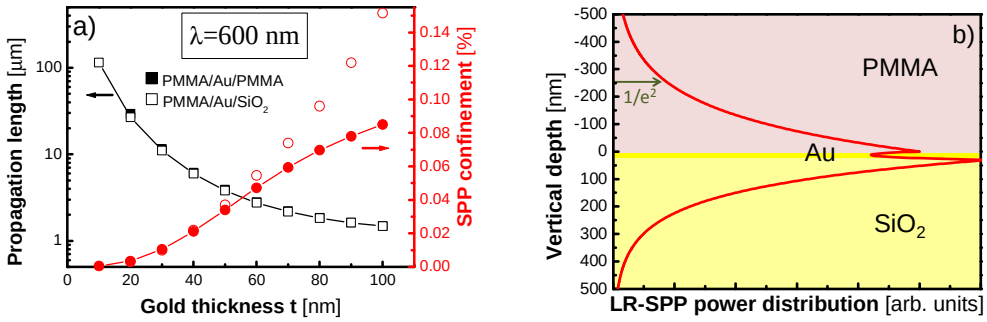

Figure 6. a) Propagation length and confinement factor dependence as a function of the gold thickness at $\lambda = 600\ nm$ b) Mode distribution at $\lambda = 600\ nm$ using $t = 30\ nm$ and the asymmetric waveguide.

b. Finite asymmetric and symmetric structures

Once the thickness of the metal was optimized, simulations using finite PMMA and SiO_2 layers were carried out. Figures 2a and 2b depicted the structures considered in this section. The bottom layers consist of 2 µm of SiO_2 on a semi-infinite Si substrate. Then, the waveguides are composed by three or four layers on SiO_2 depending on the design. In figure 2a the Au is considered to be evaporated directly onto the SiO_2 and in figure 2b there is an intermediate PMMA layer with thickness d_2. In both cases the thickness of the Au was fixed to $t = 30\ nm$, as explained in the last section. On the top of the metal a PMMA film with thickness d_1 is deposited between the metal and the air.

The PMMA layers will host QDs and other quantum nanostructures that will provide gain to the LR-SPP mode. Then it should be thick enough to contain the whole evanescent tail of the TM_0 mode. However, above a certain cladding layer thickness, higher order modes start to be guided, influencing the behavior of the amplifier. These modes are hybrid (photonic-plasmonic), because they are mostly confined in the dielectric layers (PMMA or SiO_2). Figure 7 plots the real part of the effective refractive index of the TM modes as a function of

cladding layer thickness ($d = d_1$) in the asymmetric (figure 7a) and symmetric (figure 7b) waveguides. In the second case, top and bottom PMMA layers are considered to have the same thickness ($d = d_1 = d_2$). Right axis of the figures (continuous red line) plots the propagation length of the LR-SPP mode. In both structures this magnitude increases for thin cladding films, and then it saturates above *1 μm*. In the symmetric structure (figure 7b), high order propagating TM modes are allowed for d > 700 nm and hence there will be a tradeoff between single mode operation and propagation length. In the asymmetric structure (figure 7a) the single mode threshold operation is possible up to 1.2 μm for which the propagation length saturation is reached (lowest losses).

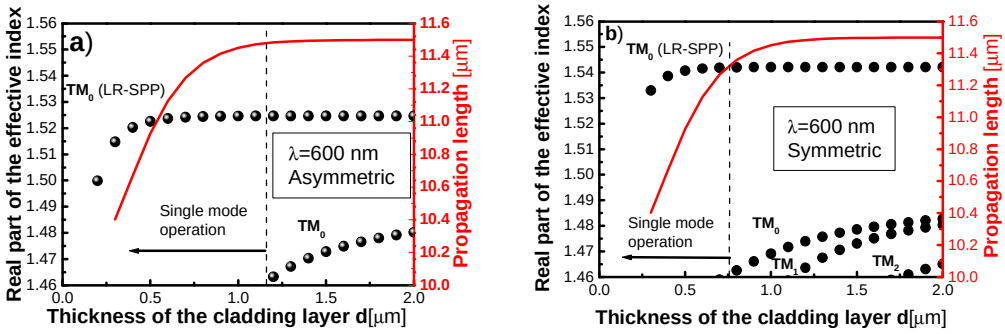

Figure 7. Real part of the effective refractive (symbols) and propagation length (red continuous line) of the TM_0 mode as a function of the cladding layer thickness for the asymmetric (a) and symmetric (b) waveguides.

As discussed above, given that symmetric and asymmetric structures give similar propagation lengths, the asymmetric one with ***d ≈ 1 μm*** is preferred because it is the simplest design and provides better mode confinements. Figure 8 shows the power distribution of the LR-SPP and the TE_0 modes (the only ones for that thickness). The first one is centered at the Au layer and the second at half of the PMMA film. However, there are also substrate radiated modes, as it is shown in table II, where all modes are listed with their corresponding effective refractive indices (N_{eff}) and propagation lengths (L_p).

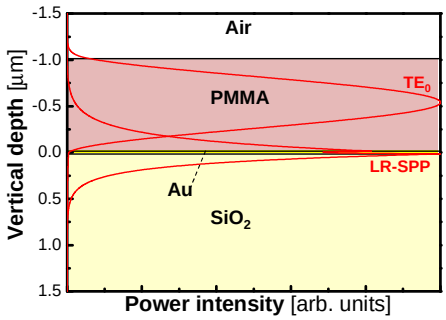

Figure 8. Power distribution of the LR-SPP mode and the fundamental TE modes in the structure.

Table II. Mode effective indexes of the plasmonic waveguide

TM			TE		
Mode	**Neff**	**Lp (μm)**	**Mode**	**Neff**	**Lp (μm)**
LR-SPP	1.5246-0.042i	11.4	**TE_0**	1.46484-0.00013	361
TM_0	1.45257-0.00068i	69.6	**TE_1**	1.45063-0.00021	225
TM_1	1.44798-0.0018i	25.6	**TE_2**	1.39234-0.0014	54.5
TM_2	1.42372-0.0082i	5.8	**TE_3**	1.39234-0.0014	33.5
TM_3	1.38739-0.0198i	2.4	**TE_4**	1.38752-0.0011	42

c. Gain effect.

The gain material chosen in this work consisted of semiconductor QDs and other quantum nanostructures embedded in PMMA. Their maximum concentration in the polymer is limited by reabsorption effects and roughness of the layers and an optimum filling factor (volume ratio of the polymer filled with QDs) $ff \sim 10^{-3}$ was experimentally determined for waveguiding applications [7]. This value is low enough to approximate the refractive index of the nanocomposite equal to that of PMMA. The following table shows the necessary net gain to be provided by the QDs to compensate for losses and to achieve a net gain of around 10 dB/cm by using the optimum thickness obtained above. First, it is interesting to note that by dispersing QDs at top and bottom of the nanocomposite, the necessary gain is halved due to the higher quantity of active centers, and the minimum material gain in the asymmetric structure is similar to the symmetric one without gain at the bottom. In literature only one reference [4] demonstrates net gain for SPP propagation, but using a very thin gold layer ($t = 4\ nm$), so that metal losses are much lower than in our designs.

Table III. Gain requirements at 600 nm

λ (nm)	**complete loss compensation**	**10 dB/cm**
600	g = 1571 cm^{-1} gain top g = 628 cm^{-1} gain top and bottom	g=1613 cm^{-1} gain top g=775 cm^{-1} gain top and bottom
1550	g = 20.3 cm^{-1} gain top g = 12.1 cm^{-1} gain top and bottom	g=40.6 cm^{-1} gain top g=20.3 cm^{-1} gain top and bottom

d. Experimental results

The design of a plasmonic amplifier requires taking into account not only the number of modes and the attenuation in the metal, but also the conditions to couple light in the waveguide and to the LR-SPP. In addition, in the case where the nanostructures are pumped optically, it is also necessary to allow an efficient excitation of them.

The structures depicted in figures 2a - b were designed with Au thickness of $t=30\ nm$ and dielectric claddings with $d = 1\ \mu m$, in order to obtain the best compromise between propagation length and mode confinement, and to provide single mode TM operation, as justified above. However, as it was shown in figure 6, the longest SPP propagation length that can be achieved at $\lambda = 600\ nm$ is only around 11 μm, making the light coupling mechanism to the LR-SPP difficult. In addition, colloidal QDs have an absorption coefficient increasing below the QD effective band-gap wavelength ($\lambda_g = 580\ nm$ for CdSe QDs), and hence efficient QD excitation should be made at wavelengths as shortest as

possible. However, at these wavelengths the ohmic losses in the gold are bigger, and in consequence the SPP suffers from higher attenuation. For example, at 405 nm the propagation length of the SPP is reduced to 0.46 µm, other than the additional attenuation by the QD absorption along the propagation of the pump beam. Indeed, in [7] we determined that nanocomposite dielectric waveguides cannot propagate the pump beam for the filling factors required for amplifications purposes (10^{-3}) [11]. This is why we focus the pump beam on the surface of the waveguides using the set-up illustrated in figure 5b. As an example, figure 9 shows the images of TE and TM modes at the wavelengths of the pump laser (404 nm, blue) and PL (600 nm, red) characterized with that experimental set-up. The sample consisted of a 30 nm Au layer evaporated on a SiO_2/Si substrate and a 1 µm thick film of CdSe-PMMA spin coated onto the metal layer. Although it should not be possible to excite the SPP at the wavelength of the pump laser (the wave vector of the incident light and the waveguide modes are orthogonal), some coupling is observed at the output of the structure under TM polarization, probably due to the roughness of the Au layer. Concerning the waveguided PL of QDs the coupling to all optical modes is possible because light emission takes place in all directions. Figure 9 shows that TE and TM (LR-SPP) modes have different intensity distribution because the first one is centered on the PMMA and the second one on the Au (see figure 8); in fact, a narrow cross section is measured for TM mode.

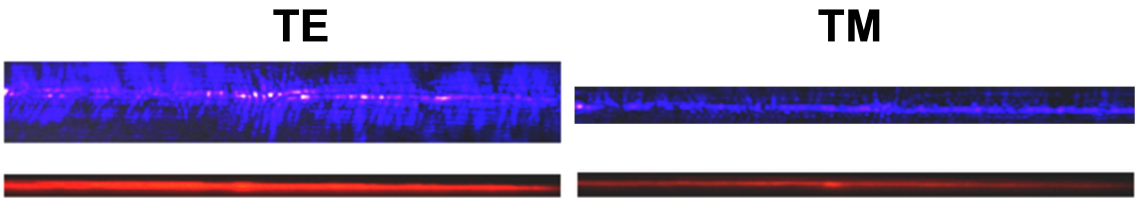

Figure 9. CCD images of the modes under TE (left) and TM (right) polarizations.

With the same experimental set-up it is also possible to estimate the gain produced by QDs and propagation losses in the structure. The method was described in section 1. Figure 10 shows the gain of the LR-SPP in samples with the structure shown in figure 2a using different filling factor of QDs in the polymer and a fixed thicknesses of $t = 30$ *nm* and $d = 1$ *µm*. PL intensity increases with the stripe length and reaches saturation for $d \approx 200\text{-}300$ *µm*. Text in figures shows the range of g_0 for fitting the experimental data by fixing $L \approx 250$ *µm (Auger losses' length)*. It is interesting to note that the higher the concentration (*ff*), the faster the slope (and hence g_0). Figure 10b shows the waveguided PL as a function of the distance between the stripe and the waveguide edge for the three samples with different *ff*. In all cases, these curves can be approximated by an exponential decay using $\alpha \approx 67$, 67 and 93 cm^{-1} for *ff = 0.0004, 0.002* and *0.008*, respectively. Similar curves were obtained under TE polarization with slightly smaller values for g_0 and α.

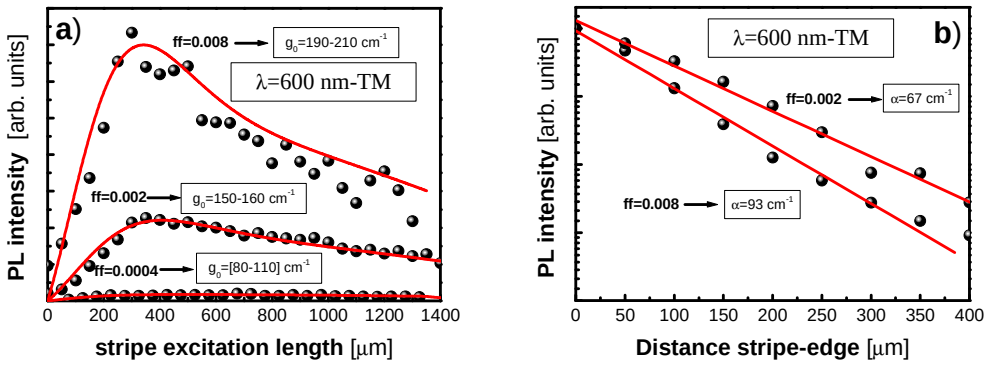

Figure 10. a) PL as a function of the stripe length. b) PL as a function of the distance between the edge of the sample and the stripe. Data refer for TM polarization.

e. Bilayer structures

The VSL method has the advantages of allowing a uniform excitation of the QDs through the waveguide and an easy set-up, but it has the drawback of a reduced pump power density (compared end-fire coupling of the waveguide). This limitation can be solved by using a thick enough PMMA cladding without QDs [12], because most of the pump beam can be coupled into the cladding with negligible absorption as compared to the nanocomposite and the metal. This alternative design is shown in figure 2c and consists of the active nanocomposite (thickness d_1) deposited onto the metal (thickness t) and a top PMMA cladding layer (thickness d_3). The structure can include a bottom PMMA cladding layer (with the same thickness d_2) between the Au and SiO_2 to build the symmetric waveguide. The idea of the pump coupling/extraction of light is shown in figure 11. First, the pumping beam is coupled into the PMMA cladding. Since most part of the mode is confined in this layer (where there is no absorption) it can propagate through the structure coupled to photonic modes in this layer (figure 11a). At the same time, the tail of the mode will overlap with the nanocomposite, exciting in consequence the QDs through the waveguide (figure 11b) [12]. Similarly, the PL can be coupled to the different waveguide photonic and plasmonic modes. Moreover, a thick cladding layer would imply the presence of high order TM modes and the signal at the output of the structure will be composed of photonic and plasmonic modes and not only by the fundamental LR-SPP. The overlap of the nanocomposite can be maximized to the LR-SPP field distribution by an appropriate choice of the thickness of the layers and, in consequence, most of the PL would be coupled mainly to the LR-SPP rather than to photonic modes (figure 11c).

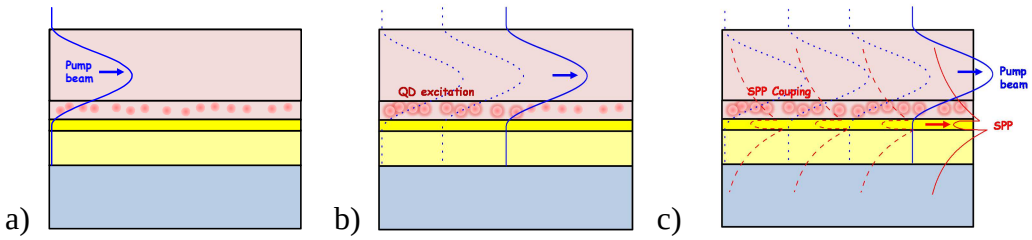

Figure 11. Plasmonic coupling through a cladding layer.

The nanocomposite thickness is fixed to ***d_1 = 250 nm*** because it is close to the evanescent tail at $1/e^2$ in the PMMA (figure 6b). Concerning the thicknesses of the bottom (d_2) and top (d_3) claddings, d_2 is set initially to zero because the asymmetric structure yields longer SPP propagation lengths. The value of d_3 will be thick enough to allow the coupling of the pumping beam and separate spatially the TM photonic modes confined in the cladding from the nanocomposite, in order to minimize the coupling of the PL to these modes. Figure 12a shows the real part of the effective refractive index and the propagation length of the photonic TE_0 and TM_1 modes at the pumping wavelength of $\lambda = 404\ nm$ as a function of the cladding thickness d_3. Since these modes are centered at the PMMA film, the thicker the cladding, the longer the gap between photonic modes and the gold, as observed in figure 12b. Therefore, due of the fact that there is no absorption in the PMMA, the propagation length increases for thicker claddings and, if $d_3 > 4\ \mu m$, the cladding acts as a semi-infinite layer for the photonic modes.

Several samples with a fixed nanocomposite and Au thicknesses of $d_1 = 250\ nm$ and $t = 30\ nm$, respectively, and different PMMA claddings ($d_3 = 0, 1.75, 5.25, 8.75\ \mu m$) were prepared in order to check the bilayer design. Figure 13 shows the estimation of the losses in the four waveguides under TE (figure 13a) and TM (figure 13b) polarizations. Losses clearly decrease with the thickness of the top cladding PMMA and give similar values for TE and TM. The unexpected value of losses with $d_1+d_3=9\ \mu m$ is possibly due to an increase of such a thick PMMA film roughness.

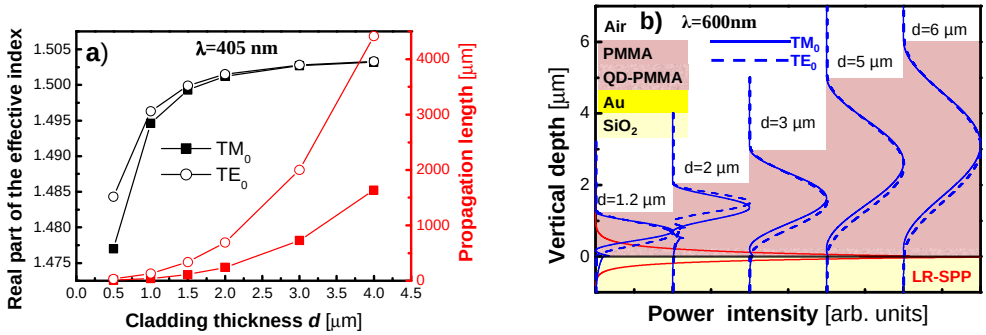

Figure 12. a) Real part of the effective index and propagation length of the TM_1 and TE_0 modes as a function of the cladding thickness d_3 using $d_1 = 250\ nm$ at $\lambda = 404\ nm$. b) Mode distribution at $\lambda=600\ nm$ with different cladding thicknesses.

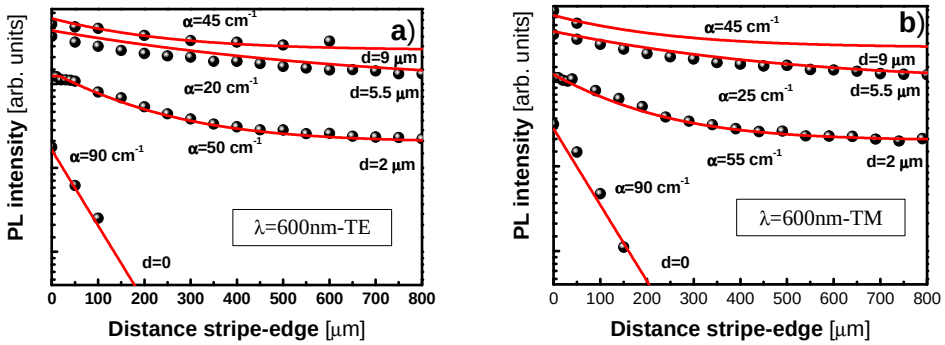

Figure 13. PL as a function of the distance between the edge of the sample and the stripe under TE and TM polarizations for different cladding layer thicknesses.

For thick cladding layers it is possible to couple the pump beam from the edge of the sample (figure 14a). The characterization of a sample with $d = d_1+d_3 = 5.5\ \mu m$ was carried out by using the set-up of figure 14a and a 533 nm pumping laser. In figure 14b the top panels plot the images of the waveguided PL under TE and TM polarizations and the bottom panels their corresponding intensity profiles along the vertical cross section. Clearly, the TM intensity profile has a cross section thinner than the TE one and hence, by comparing to the mode distributions shown in figure 12b, it is reasonable to associate the first to the LR-SPP mode.

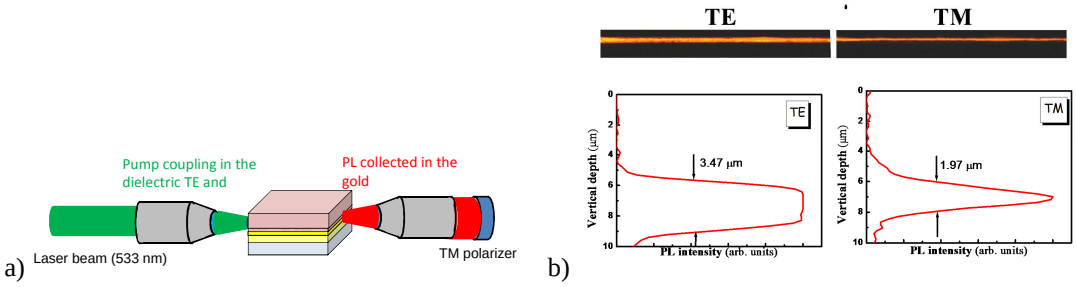

Figure 14. a) End fire coupling experimental set-up. b) Characterization of the mode distribution in a sample with $d_1+d_3=5.5\ \mu m$.

3. Design of planar plasmonic amplifiers at 1550 nm.

In this section we will extrapolate main conclusions obtained at $\lambda = 600\ nm$ to the infrared region and specific results.

a. Three-layer structures

As a first step in the simulations, PMMA/Au/PMMA and PMMA/Au/SiO_2 structures using semi-infinite PMMA and SiO_2 dielectric layers were initially simulated. Figure 15a shows the propagation length and the confinement factor at $\lambda = 1550\ nm$ calculated for both structures. At this wavelength the propagation length can reach the mm range while the mode confinement reduces down to 0.05 % for $t = 30\ nm$. The symmetric structure (PMMA/Au/PMMA) presents lower losses and larger propagation length than the asymmetric one (PMMA/Au/SiO2). Moreover, it is important to mention that the asymmetric waveguide does not show propagating modes for Au layers thinner than 60 nm. Again, a good compromise for the thickness of the layer is $t = 30\ nm$. Figure 15b plots the mode distribution of the LR-SPP mode in the symmetric PMMA/Au/PMMA waveguide using $t = 30\ nm$. The mode is centered in the metal and the evanescent tail extends to 2 µm at $1/e^2$, one order of magnitude larger than that calculated at $\lambda = 600\ nm$.

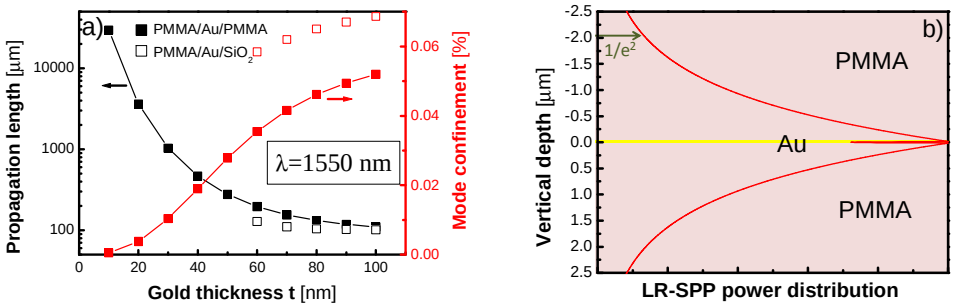

Figure 15. a) Propagation length and confinement factor as functions of the gold thickness (*t*) at *λ= 1550 nm* b) Mode distribution at *λ= 1500 nm* using *t=30 nm* and the asymmetric waveguide.

b. Finite asymmetric and symmetric structures

Simulations with finite claddings have been carried out in both the symmetric and asymmetric waveguide. Figure 16a shows the real part of the effective refractive index as a function of the cladding thickness (d_1). The waveguide presents single-mode operation for claddings thinner than 4 μm, but the propagation length of the TM_0 mode is very small (the structure cannot propagate the LR-SPP, as was shown in figure 15a). This mode exhibits a hybrid photonic-plasmonic nature extended in the PMMA and the SiO_2, as observed in figure 16b, dominating the plasmonic nature for d < *1.5 μm*. For *d > 3 μm* the mode has a negligible distribution at the metal, losing its plasmonic nature. Moreover, red line of figure 16a shows that the propagation length has an exponential increase with *d*, instead of the saturation for thick claddings usually observed for the LR-SPP. The TE_0 mode has a quasi-Gaussian distribution centered on the PMMA for *d > 1 μm*, whereas for *d < 1 μm* the cladding is too thin to guide any propagating mode, and the solution is a radiated mode centered at the SiO_2 bottom layer, as shown in figure 16b.

The symmetric structure (figure 2b) can propagate the LR-SPP at *λ = 1.55 μm*. Nevertheless, a careful design of the waveguide should take in account the thicknesses d_1 and d_2, because they have an implication in the shape of the mode. Figure 17a shows the real part of the effective refractive index and the propagation length of the LR-SPP as a function of the cladding thicknesses, considering the same thickness on top and bottom sides of the Au layer ($d = d_1 = d_2$). The waveguide is single mode for d < *3 μm* and propagation length increases with the cladding thickness and saturates to 1.1 mm for *d > 4.5 μm*. Figure 17b plots the power mode distribution of the LR-SPP, TM_1 and TE_0 modes for different values of *d*. The LR-SPP mode is asymmetric for thin layers due to the refractive index mismatching, but it gets a symmetric distribution when the layer is thick enough to keep the evanescent tail (*d >3 μm*). The waveguide has photonic propagating TE modes for *d > 1.5 μm*, but the power intensity distribution of both the fundamental TE_0 and the first order TM_1 modes tend to be concentrated at the bottom cladding layer.

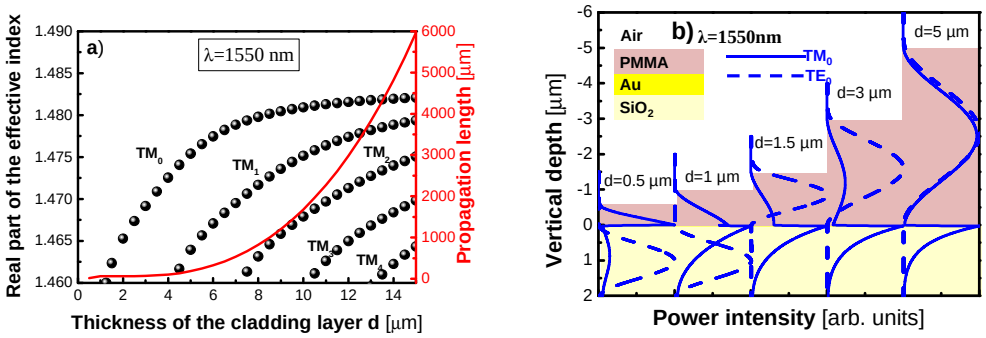

Figure 16. a) Real part of the effective refractive index (symbols) and propagation length for the TM_0 mode (red line) as a function of the cladding layer in the asymmetric structure at 1550 nm. b) Mode distribution for different cladding thicknesses.

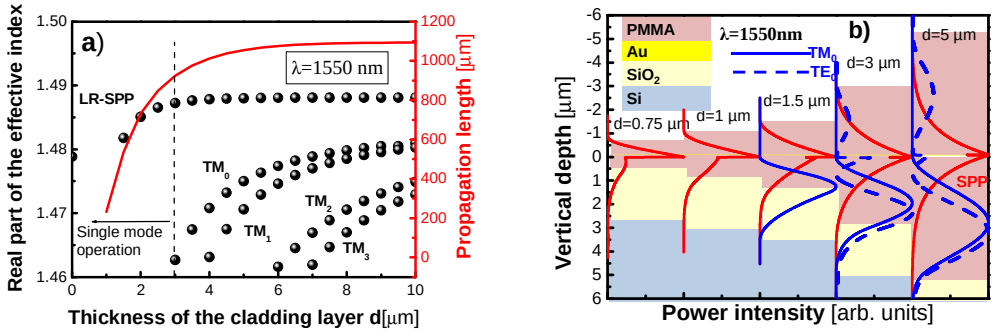

Figure 17. a) Real part of the effective refractive index (symbols) and propagation length of the TM_0 mode (red line) as a function of the cladding layer in the symmetric structure at 1550 nm with $d = d_1 = d_2$. b) Mode distribution for different cladding thicknesses.

The symmetric structure can allow the propagation of the LR-SPP at *1.55 μm* with an extensive evanescent tail (see figure 17b) and high order TM hybrid modes appears for thick cladding layers. A good compromise would be to consider a partial symmetric structure with $d_2 = 2\ \mu m$ and vary the top cladding thickness (d_1). Figure 18a shows the real part of the refractive index (symbols) and the propagation length (red line) as a function of d_1. The waveguide can achieve single mode operation for $d_1 < 4\ \mu m$. Propagation length saturates to around 0.9 mm for $d_1 > 4\ \mu m$. Figure 18b shows the mode distribution of the LR-SPP, TM_1 and TE_0 modes. For thin claddings ($d_1 < 1.5\ \mu m$) fundamental TM_0 mode has a hybrid plasmonic-photonic nature (although it is plotted in the figure as the LR-SPP for a better understanding), but for thicker top cladding layers the structure can propagate the LR-SPP with a symmetric distribution. The photonic TE_0 and TM_1 (appearing for 3 and 5 μm) modes are concentrated at the bottom PMMA for $d_1 < 1.5\ \mu m$ and at the top layer above that thickness.

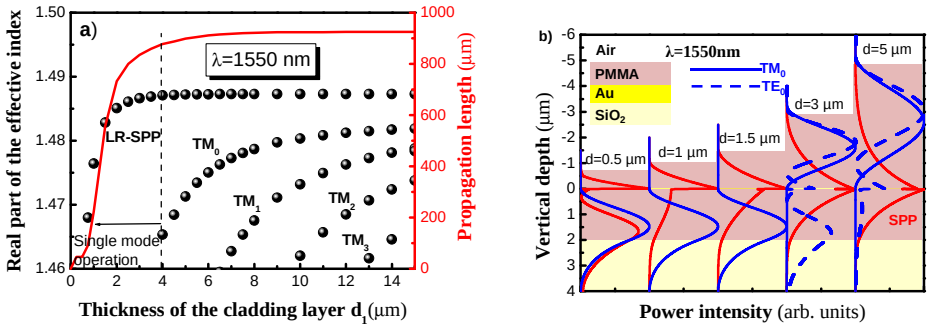

Figure 18. a) Real part of the effective refractive index (symbols) and propagation length of the TM_0 mode (red line) as a function of the top cladding layer (d_1) in a partially symmetric structure at 1550 nm setting $d_2 = 2\ \mu m$. b) Mode distribution for different values of d_1.

c. Gain effect.

Losses can be compensated at $\lambda = 1.55\ \mu m$ with weaker requirements than they were at $\lambda = 600nm$. Table III shows the necessary gain to compensate losses completely and to obtain a net gain of 10 dB/cm for the LR-SPP propagation, considering $d = 2\ \mu m$. The required gains reduce to values of the order of 10 – 20 and 20 – 40 cm^{-1} to compensate and get amplification, respectively. The gain generation at $\lambda = 1.55\ \mu m$ will be possible by using QDs with emission in the IR, like those based on PbS and PbSe materials. Again, the filling factor of QDs in the polymer is set to the range of 10^{-3} in order to allow a good dispersion, as it was explained above. In addition, it is useful that QDs exhibit a high Stokes shift in order to avoid self-absorption of the PL, which is possible by the use of core-shell PbS-CdS PER Quantum Rods (QR) from UGent. These nanostructures have a broad band of emission in the IR with the absorption edge at 450 nm and preliminary characterization yielded gains ≈ 300 cm^{-1}.

d. Bilayer structures

The structure shown in figure 2c can be used to improve the coupling of the pumping beam as it was explained in section 2e. When the asymmetric waveguide is considered, the top thickness of the cladding layer has to be set to only ≈ 1 µm in order to maximize the plasmonic nature of the TM_0 mode (see figure 16b), and hence a bilayer waveguide based on this design is not a good choice. The symmetric waveguide could be a good option to design the bilayer structure on the top of the gold. Moreover, it was discussed above that there is a cross-talk between optical losses and single mode operation of the plasmonic structure at $\lambda=1550\ nm$, because the cladding has to be thicker than 5 µm to keep the whole evanescent field of the LR-SPP and minimize losses. However, high order TM modes will appear for such a thickness, a problem that can be solved by designing properly the bilayer structure (figure 2c), as was considered in figure 18.

The thickness of the nanocomposite (d_1) should have a good overlap with the mode distribution of the LR-SPP in order to provide it gain. Here it is important to take into account that the LR-SPP has an evanescent decay across the dielectric layers. Then, although the evanescent field is around 5 µm, most of the mode power is in the first 1.5 µm from the gold

(Full Width at Half Maximum is around 1.4 µm), and hence a good value for the nancomposite thickness (d_1) should be close to this value. Concerning the top cladding layer (d_3), it has to be thick enough to contain the evanescent tail of the LR-SPP, and then a value of d_3 = *4-5 µm* would be a good option. Although with such a thickness, high order propagating TM modes are allowed, they will be centered at the top cladding PMMA (see figure 18b). As a consequence, the overlap of these modes with the nanocomposite will be strongly reduced and hence the coupling of the PL to these modes will be minimized.

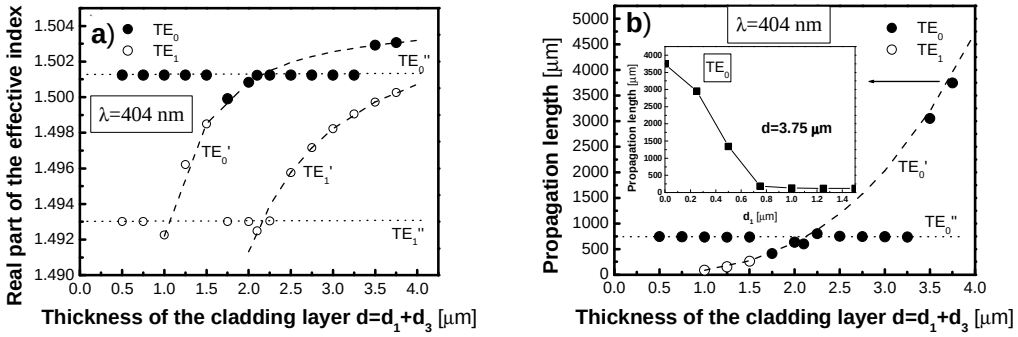

Figure 19. a) Real part of the effective refractive index of TE_0 an TE_1 photonic modes as a function of the thickness of the cladding layer ($d = d_1+d_3$) setting $d_2 = 2\ \mu m$. Superscripts ' and '' refer to the effective refractive indices of the top and bottom cladding layers. b) Propagation length as a function of *d*. The inset shows the decrease of propagation length because of the attenuation in the nanocomposite.

Moreover, the claddings can be also optimized to couple the pumping beam (at 404 nm) from the edge of the sample in the same way as it was explained in section 2e. It is important to take into account that the bottom and top cladding layers act as independent waveguides for the photonic modes. Then, light can propagate in both layers, and for thin enough gold thicknesses it can be coupled from one waveguide to another [13]. Black and white symbols of figure 19a shows the effective refractive index of the fundamental (TE_0) and first order photonic modes (TE_1) as a function of the top cladding layer ($d = d_1+d_3$) setting $d_2 = 2\ \mu m$. Dotted lines refer to the first two TE photonic modes (TE_0'' and TE_1'') that can propagate in the bottom PMMA cladding when $d = 0$ and $d_2 = 2\ \mu m$. Similarly, dashed lines show the effective refractive indices of the first two TE photonic modes (TE_0' and TE_1') propagating in the asymmetric structure ($d_2 = 0$). For thin cladding layers ($d < 1\ \mu m$) the top waveguide cannot support any propagating mode and all light is guided by the bottom PMMA. Indeed, the real part of the effective refractive index increases with *d* in the same way it did in the asymmetric structure and the effective refractive indices of the top and bottom layers become equal for $d = 2\ \mu m$. Above this thickness light turns to be coupled to the top layer. Propagation length of the fundamental mode has a similar behavior, as shown in figure 19b, and *d* has to be set between 3 and 4 µm. Concerning the exact value of d_1 and d_3, initial designs could be $d_1 = 1.5\ \mu m$ and $d_3 = 4\ \mu m$ in order to maximize the overlap of the active centers with the LR-SPP and to avoid the coupling of the PL to high order TM modes. However, here it is important to calculate the absorption of the pump beam produced in the nanocomposite. The inset of figure 19b shows the propagation length as a function of d_1 setting $d = 3.75\ \mu m$ and considering an absorption in the nanocomposite of around 30 cm^{-1} (the one estimated with a filling factor of 10^{-3} at $\lambda = 404\ nm$). The thicker d_1 the higher PL and for $d_1 > 1.5\ \mu m$ there is no propagation. Experimentally, samples have to be thicker than 1-2 mm in order to be handled, and a value of $d_1 = 0.5\ \mu m$ has been chosen. Finally, it is

interesting to say that TM shows a similar behavior with less propagation length, so polarization TE should be chosen to pump the waveguides.

e. Preliminary results

Samples with the asymmetric (figure 2a) and symmetric (figure 2b) structures were fabricated setting $d_1 = d_2 = 2\ \mu m$ using nanocomposites made by the dispersion of PbS QDs in PMMA. Figure 20 shows the characterization of the losses with the VSL method of the bilayer structure. Symbols and continuous lines correspond to experimental data and their corresponding exponential fitting, respectively. The highest losses are measured for TM polarization that suggests its identification with the LR-SPP. Indeed, the top panels of the figure show images of the waveguided light in both polarizations, where we see a narrower distribution for TM, as was shown in figure 18b.

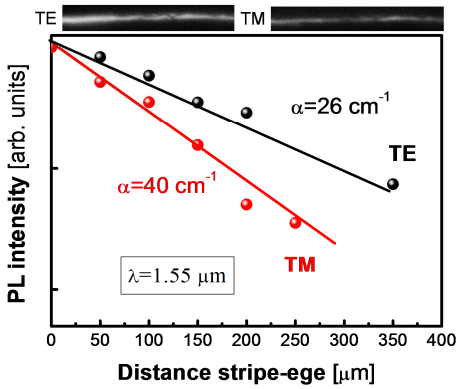

Figure 20. PL intensity as a function of the distance between the stripe and the edge of the sample under TE (black) and TM (red) polarizations. Top panels show IR-CCD images of these modes.

Figure 21 shows the characterization of asymmetric waveguides made by the dispersion of PER QRs in PMMA with $d = 1.5\ \mu m$ using samples with two different filling factors. Figure 21a plots the PL as a function of the distance between the stripe and the edge of the sample. PL increases with the length of the stripe and saturates for $x = 400\ \mu m$. It is interesting to note that PL intensity and associated gain increases strongly with the concentration of nanoparticles in the polymer. Concerning the losses, figure 21b plots the PL intensity as a function of the distance between the stripe and the edge of the sample. The decay is around 50 cm^{-1} and seems to be similar for both concentrations because these QRs

have a large Stokes shift.

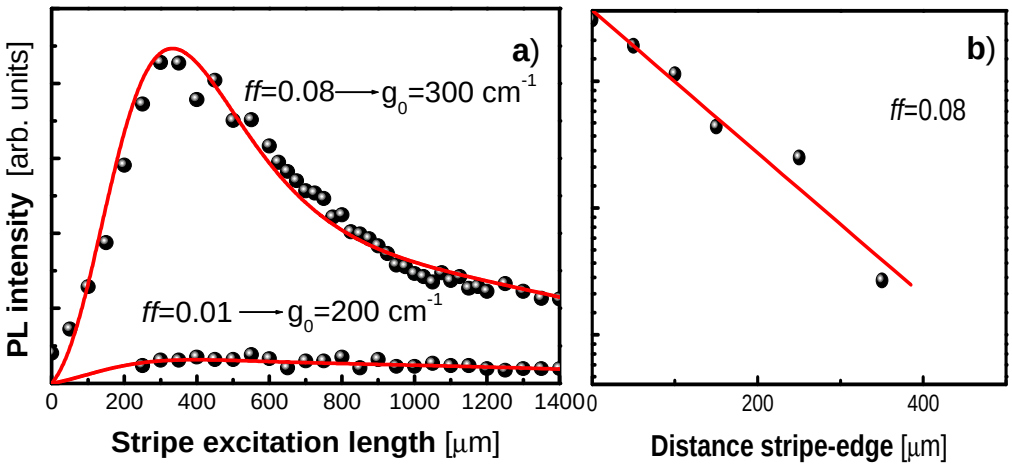

Figure 21. a) PL intensity as a function of the stripe excitation length in sample with two filling factors with PER QRs. b) PL as a function of the distance between the stripe and the edge of the sample. Red continuous line shows the fitting of the curves.

In order to allow the waveguides for end fire coupling, samples with the bilayer structure (figure 2c) were fabricated using the asymmetric structure, setting the value of *ff* to 10^{-3}. Figure 22 shows the losses characterization with the VSL method in TE (figure 22a) and TM (figure 22b) for samples for different cladding layers $d_3 = 0, 1, 5.5$ *and* $10\ \mu m$ and $d_1 = 1\ \mu m$. Losses are always bigger in TM than TE because of the fact that there is more influence of the gold (influence of LR-SPP mode). It is important to note that the larger d_3, the smaller the losses because propagation is dominated by photonic modes centered at the dielectric. For $d_3=0$ losses have a value smaller than expected. Concerning the end fire coupling characterization, a minimum thickness of about 3 μm is necessary to allow the propagation of the pump beam through the structure. Also, with this kind of nanocrystals it is important to limit the value of d_1 in order to avoid reabsorption effects. In these conditions, figure 23a shows an image of the waveguided PL in a sample with $d_1 = 0.5\ \mu m$ and $d_3 = 3\ \mu m$, coupling at the edge of the sample a 533 nm laser. Clearly, TM distribution is narrower, probably due to the influence of the gold. Similar findings are observed for the symmetric structure with $d_1 = 0.7\ \mu m$, $d_3=2.3\ \mu m$ and $d_2=2\mu m$ (figure 23b).

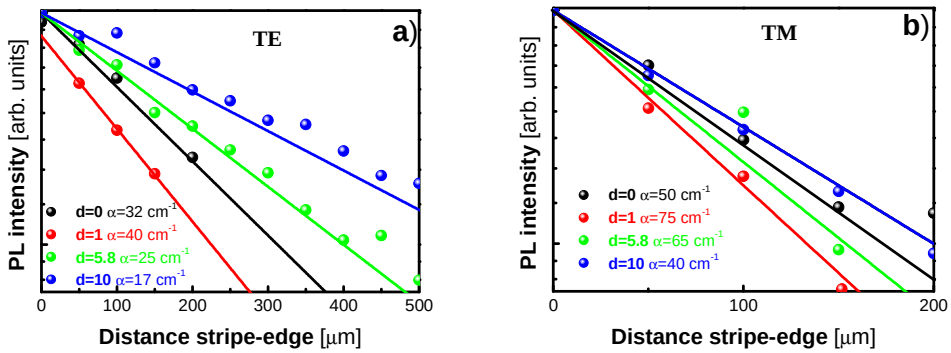

Figure 22. a) PL intensity as a function of the stripe excitation length in samples with a bilayer asymmetric structure in TE (a) and TM (b) polarizations.

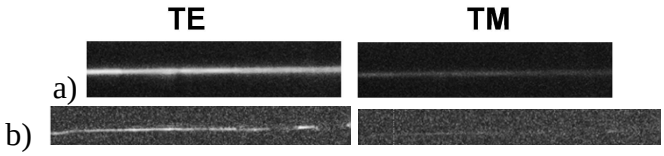

Figure 23. Images with a IR-CCD camera of asymmetric (a) and symmetric (b) bilayer structures under TE and TM polarizations.

4. Two dimensional amplifiers

Two dimensional amplifiers with the structures shown in figure 3 are planned to be prepared and fabricated in the next months of the project. These structures have the advantage, with respect to the planar ones, of a better confinement of the mode, an easier integration with other devices and smaller losses. Then, the optimization of the device parameters developed in this deliverable will be extended to this 2-D waveguides, and the structures will be fabricated and characterized. Figure 24 shows preliminary results considering a 1 µm PMMA pattern on top of the gold layer at 600 nm (dielectric loaded 2D waveguide).

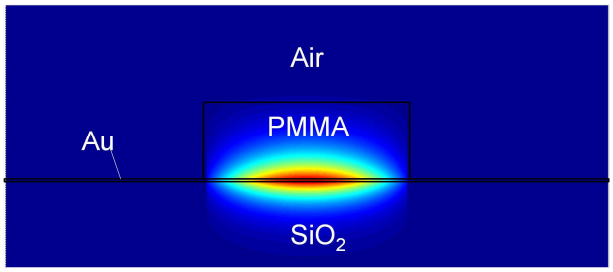

Figure 24. Fundamental TM00 mode profile at 600 nm considering a 1 µm PMMA pattern on a gold film.

5. Design of hybrid silicon-plasmonic amplifier

The goal of this task is to determine a final structure for the plasmonic amplifier on the silicon-on-insulator (SOI) platform. The idea is to leave the existing high-performance SOI

framework (which inherits its excellence in large from highly advanced CMOS fabrication) unaltered, but rather extend it. In this view, we propose a hybrid platform where standard SOI waveguides are covered with an active layer (e.g. for modulation or light generation) and a cathode layer (for electrical contacting). Since silicon is conducting (or can be made so by p/n-doping) we can use the waveguide itself as the anode contact. Such a generic structure is shown in figure 25.

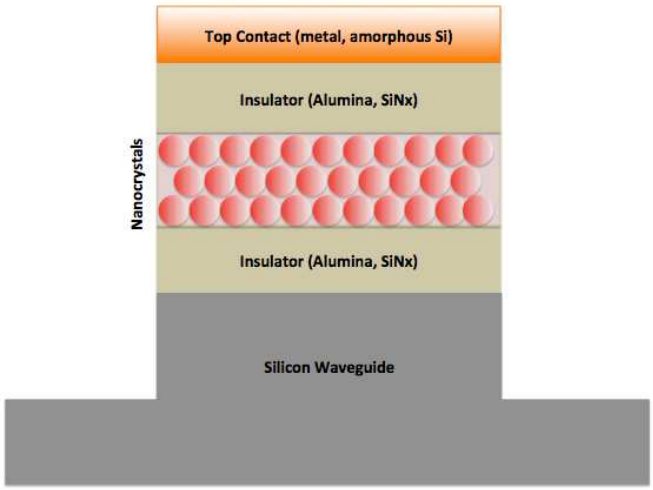

Figure 25: Generic structure for integrating a nanocrystal light source on silicon.

We propose to use gold or amorphous silicon as the cathode material. Gold is suggested as it is the most stable of the alternatives such as Ag and it shows better plasmonic confinement with lower loss (compared to e.g. Al). Alternative materials such amorphous silicon (a:Si) could be viable candidates. However, the technology is not yet optimized in our labs and moreover it is not clear whether a high temperature PECVD process (for poly-Si) or any other type of plasma deposition will conserve the optical properties of the nanocrystals. Simple DC plasma sputtering of Alumina on nanocrystals seems to suggest this hypothesis. Nonetheless, we include a:Si in our simulations to investigate this alternative. The silicon waveguide used as the anode can be configured as a wire, a ridge or a slab.

To summarize, the main advantages of our proposed structure are:

- Generic platform (not only nanocrystals can be embedded, also other luminophores)
- Broadband (no spectral features) and low-cost
- Possibility for both electrical and optical excitation
- *High mode confinement with acceptable propagation loss*
- *Processing compatible with nanocrystals & CMOS compatible*

We will elaborate on points 4 and 5 concerning the optical properties and the feasibility of real device fabrication.

High mode confinement with acceptable propagation loss

Simulations are carried out using the finite-element modeling (FEM) tool COMSOL 3.5. We can input the optical parameters of the different layers at a given wavelength and obtain the mode profile (for calculating mode confinement) and the effective refractive index of the mode (for propagation length). Since we focus on light emission and absorption around

telecom wavelengths (e.g. 1550 nm) we can limit ourselves to quantum nanostructures with effective bandgap in those spectral regions. Both silicon slab, ridge and rib waveguide geometries are investigated. The ridge waveguide has a shallow etch depth of 70 nm leading to a 150 nm ridge. The rib geometry has a fully etched 220 nm trench. Refractive indices for silicon and silica at 1550 nm are taken to be 3.445 and 1.445 respectively.

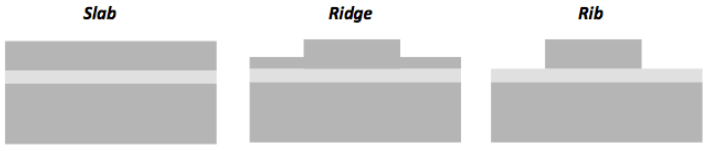

Figure 26: Different waveguide shapes considered

A crucial step is the model used for the nanocrystal layer itself. We obtained the optical constants of nanocrystal multilayers around the bandgap emission from a detailed analysis of the absorption of standard silicon waveguides covered with nanocrystals [14]. The optical constants for a triple layer of colloidal nanocrystals emitting at 1550 nm are shown in figure 27 (left). Since the electrical excitation mechanism (see MS21) requires multilayers (at least 3 layers based on the proposed mechanism), we can limit our modeling to stacks thicker than a triple layer (i.e. 24 nm). The insulating layers are chosen to be 50 nm thick.

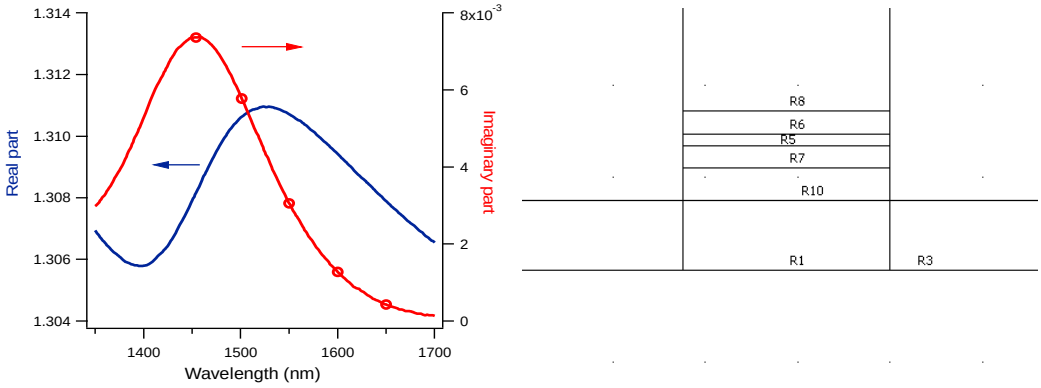

Figure 27: (left) Optical constants of nanocrystal layer (3 monolayers) and (right) geometrical model used as input for the FEM model. The nanocrystal slot region is denoted as R5.

The ground mode of the structure is evaluated in terms of two parameters: the mode confinement Γ and the propagation length L. The latter is related to the absorption coefficient of the mode as $L = \frac{1}{\alpha}$ and is calculated as:

$$L = \frac{\lambda_0}{4\pi n_{eff,i}}$$

where $n_{eff,i}$ is the imaginary part of effective mode index.

The confinement factor expresses how much of the guided mode is confined in the nanocrystal layer (denoted A) by means of the following expression:

$$\Gamma = \frac{n_A c \varepsilon_0 \iint_A |\boldsymbol{E}|^2 dxdy}{\iint_\infty \Re e(\boldsymbol{E} \times \boldsymbol{H}^*) \cdot \mathbf{1}_z dxdy}$$

This expression is a modified form of the classical 'power confinement' – expression and is more accurate for structures with high index contrast.

Combining both quantities, we can calculate the transparency gain in absence of mirror loss:

$$g_{th} = \frac{\alpha}{\Gamma}$$

Below the lasing threshold, the emission will be dominated by spontaneous emission. Coupling of spontaneous emission to the lasing mode will help lower pumping rates. The coupling is expressed through the Purcell factor, which can be calculated for 2D structures as:

$$F_{2D} = \frac{3}{4\pi}\frac{c/n}{v_g}\frac{(\lambda_0/n_{eff})^2}{A_{eff}}$$

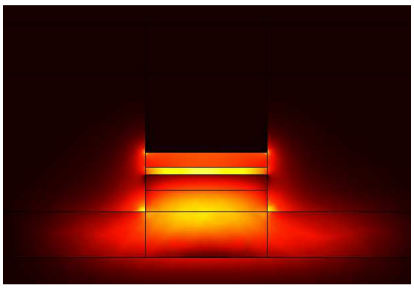

Figure 28: Typical mode profile (In plane-Power Flow) of the ground mode for a hybrid waveguide consisting of a ridge waveguide and a top metal contact).

The simulations (see figure 29) show that the propagation length and mode confinement are mainly a function of the thickness of the active region. The optical parameters show only a weak dependence on the waveguide width.

Table IV summarizes the typical parameters for the different hybrid waveguide configurations. It is clear that the structure with a:Si as top contact shows the best performance, especially in terms of transparency gain required for a low threshold optical amplifier. However, this structure is not truly plasmonic in nature so we also consider the metal-contacted structures. In these configurations, the material gain required is close to 2000 cm^{-1}, a value typical for III-V compounds. The question still remains whether this is achievable using colloidal nanocrystals however (see also D4.2).

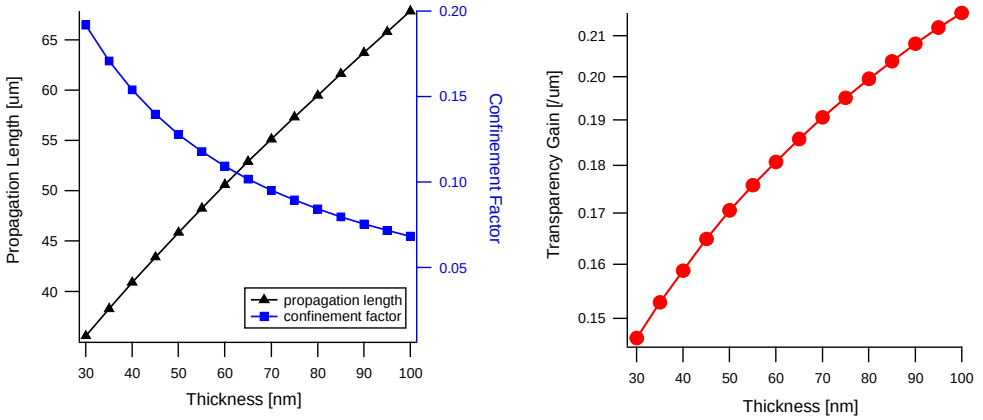

Figure 29: Simulation output (at 1550 nm) for hybrid Au/Silicon waveguide depicted in figure 3; (left) Propagation length and confinement factor and (right) transparency gain for varying slot thickness.

Typical gain cross sections at telecom wavelengths for lead-chalcogenide nanocrystals are in the order of $10^{-15} cm^2$, leading to maximal (material) gain values of 1500 cm^{-1}. This indicates that achieving optical gain in these hybrid waveguides will be very difficult unless either a:Si or novel nanocyrstals with higher gain cross section are used.

Top Cathode	Au	Au	a:Si
Bottom Anode	Si Slab	Si-ridge	Si wire
Confinement Γ(%)	6.84	7.33	4.93
Optical Loss (dB/cm)	0.6	0.6	0.003
Transparency gain (1/cm)	2130	1940	18
F_{2D}	6.5	7.1	5.84

Table IV: Typical parameters for different cathode/anode combinations of the hybrid waveguide with a 50 nm insulator thickness

Proposed processing scheme

Starting from an SOI wafer, the following processing steps are required:

- Ohmic contact formation to silicon
- Insulator deposition using ALD (Atomic Layer Deposition)
- Nanocrystal deposition
- Insulator deposition using ALD
- Cathode deposition using thermal evaporation of Au or PECVD of a:Si.

All of these steps are CMOS compatible and the steps following the ohmic contact formation can happen at low temperature (<150 °C) to avoid damaging the nanocrystals. The technology to carry out these steps (from metal to insulator depositions, lithography, …) are available in the IMEC cleanroom in Ghent. Questions remain open on a:Si as to whether it will conserve the nanocrystal properties and provide sufficient electrical stability under high AC voltages. This is currently under investigation.
The silicon waveguides required have been fabricated. The masks for further processing are available (see Figure 30 & 31)

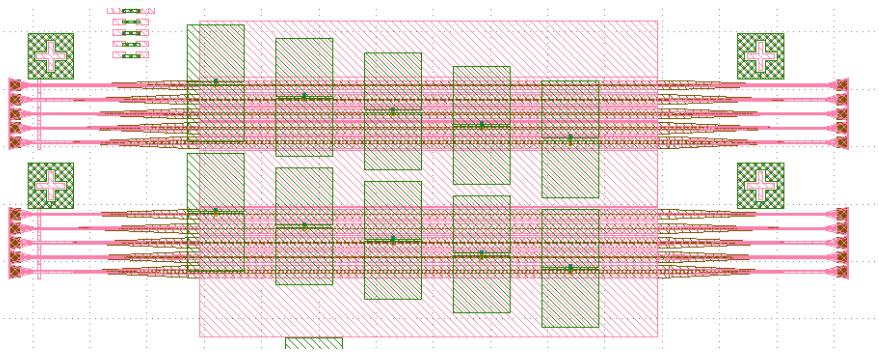

Figure 30: Layout of contact mask for device fabrication. The SOI waveguides are depicted in pink and the device contact area is depicted in green.

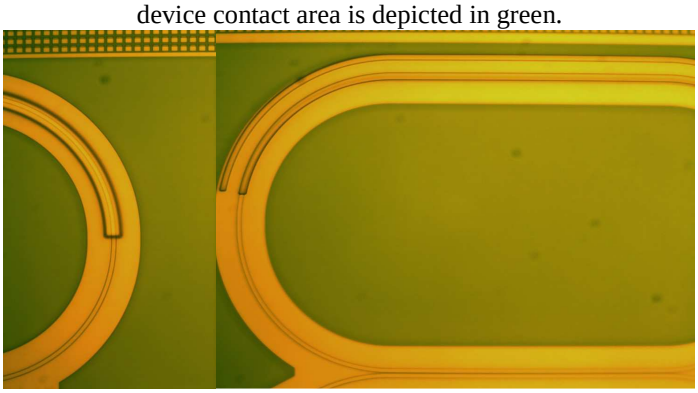

Figure 31: Lithographically defined device area on SOI ring resonators

6. Conclusions

This report deals with the design of planar plasmonic amplifiers based on QD-PMMA nanocomposite and silicon-plasmonic heterostructure. Due to the fact that work at 1550 nm is particularly challenging and most of the literature is focused on CdSe QDs, the initial wavelength studied in the QD-PMMA device was 600 nm. Once the optimum design and basic fabrication parameters have been tested at this wavelength, they have been extrapolated at IR wavelengths. Moreover, preliminary experimental results at both wavelengths have been included in the report and different kinds of colloidal quantum nanostructures have been tested, concluding that the best ones in terms of amplification are colloidal quantum rods because of their large Stokes shift. Three different planar structures were thoroughly studied, and it has been concluded that for IR wavelengths a symmetric (PMMA/Au/PMMA) with a bilayer cladding on the top is optimum to propagate the LR-SPP and to couple the pump beam. Therefore, this kind of structures is considered to be an optimal design for the plasmonic amplifier. Our next steps will be to continue working with this waveguide in order to test the amplification or loss compensation with colloidal QRs. Then, the objective is to move to 2D waveguides with patterns of polymer on the gold and with metal stripes. For this purpose, a 2D effective index method is under development with the intention to complete the design of short foot-print and more efficient plasmonic amplifiers.

Also, for the hybrid silicon-plasmonic amplifier structures optimal designs were derived. It is shown that it is advantageous to keep the thickness of the gain layer as thin as possible, because this increases the confinement in the active layer in a superlinear way. The closely packed qdot-layer allows exploitation of enhanced absorption/gain due to dipole-interactions in the QDOT superlattice. These structures are currently being fabricated. This structure has the advantage of providing a built-in approach for electrically injecting the QDOT-layer. The currently most robust approach consists in applying an AC-voltage over an insulating layer stack, but the design is compatible with approaches based on direct current injection also.

7. References

[1] D.K. Gramotnev and S.I. Bozhevolnyi, "Plasmonics beyond the diffraction limit", *Nature Photonics* **4**, 83-91 (2010).
[2] P. Berini, "Long-range surface plasmon polaritons", *Advances in Optics and Photonics* **1**, 484-588 (2009).
[3] I. De Leon and P. Berini, "Amplification of long-range surface plasmons by a dipolar gain medium", *Nature Photonics* **4**, 382-387 (2010).
[4] M.C. Gather, K. Meerholz, N. Danz and K. Leosson, "Net optical gain in a plasmonic waveguide embedded in a fluorescent polymer", *Nature Photonics* **4**, 457-461 (2010).
[5] M. Ambati, S.H. Nam, E. Ulin-Avila, D.A. Genov, G. Bartal and X. Zang, "Observation of stimulated emission of surface plasmon polaritons", *Nanoletters* **8**, 3998-4001 (2008).
[6] J. Grandidier, G. Colas des Francs, S. Massenot, A. Bouhelier, L. Markay, J.C. Weeber, C. Finot and A. Dereux, "Gain-assisted propagation in a plasmonic waveguide at telecom wavelength", *Nanoletters* **9**, 2935-2939 (2009).
[7] I. Suárez, H. Gordillo, R. Abargues, S. Albert and J. Martínez-Pastor, "Photoluminiscence waveguiding in CdSe and CdTe QDs-PMMA nanocomposite films", *Nanotechnology* **22**, 435202 (2011)
[8] H. Gordillo I. Suárez, R. Abargues, P. Rodríguez-Cantó, S. Albert and J.P. Martínez-Pastor, "Polymer/QDs nanocomposite for waveguiding applications" *Journal of Nanomaterials*, **2012**, 960201 (2012)
[9] H. Gordillo I. Suárez, R. Abargues, P. Rodríguez-Cantó and J.P. Martínez-Pastor, " Color tuning and white light by dispersing CdSe, CdTe and CdS in PMMA nanocomposite waveguides", IEEE Photon. J. **5**, 2201412 (2013).
[10] G. Lifante, "Integrated Photonics. Fundamentals", ed. John Wiley & Sons, 2003.
[11] V. I. Klimov, "Nanocrystal quantum dots: from fundamental photophysics to multicolor lasing", *Los Alamos Science* **28**, 214-220 (2003).
[12] H. Gordillo, I. Suárez, R. Abargues, P. Rodríguez-Cantó, G. Almuneau and J.P. Martínez-Pastor, "Quantum-dot double layer polymer waveguides by evanescent light coupling", *IEEE Journal of Lightwave Technology*, submitted.
[13] P. Andrew and W.L. Barnes, "Energy transfer across a metal film mediated by surface plasmon polaritons", *Science* **306**, 1002-1005 (2004).

[14] A. Omari e.a.,"Light absorption in hybrid silicon-on-insulator/quantum dot waveguides", submitted to Optics Express.